Activator–Mediator binding stabilizes RNA polymerase II orientation within the human Mediator–RNA polymerase II–TFIIF assembly

Carrie Bernecky[1,2] and Dylan J. Taatjes[1*]
[1]*Dept. of Chemistry and Biochemistry, University of Colorado, Boulder, CO 80309 USA.*
[2]*Present address: Ludwig-Maximilians University, Munich, Germany.*
**Corresponding author. Email: Taatjes@colorado.edu; Phone: 303 492-6929; Fax: 303 492-5894*

Supplemental Information

Supplemental Figure and Table legends

Supplemental Fig. 1. Negative-stain EM reconstruction of activator-free Mediator–pol II–TFIIF. (A) Representative micrographs shown in untilted and tilted stage orientations. (B) Different views of the 3D model of activator-free Mediator–pol II–TFIIF, rendered at 1.8 MDa. (C) Angular distribution of single-particle images within the Mediator–pol II–TFIIF negative stain data set. (D) Correlation curves corresponding to different resolution measures.

Supplemental Fig. 2. Cryo-EM and image processing information for Mediator–pol II–TFIIF. (A) Micrograph (B) Power spectrum from the micrograph shown in A. Micrographs were excluded from the data set if they displayed evidence of astigmatism or sample stage drift. (C) Angular distribution of single-particle images within the cryo-EM data set. (D) Resolution plot for the cryo-EM reconstruction of Mediator–pol II–TFIIF.

Supplemental Fig. 3. Structural models of the human PIC. (A) For comparison, the "front" and "side 1" views of the VP16-Mediator–pol II–TFIIF assembly is shown.[1] Note that this orientation appears most compatible with transcription initiation (see text). In the Side 1 view, the "X" denotes the pol II stalk domain (RPB4/7) protruding from the structure. The locations of TFIIA, TFIIB, TFIID, TFIIE, TFIIF, and TFIIH are based upon previous biophysical and functional studies.[2-10] (B) and (C) Structural models for the two predominant pol II docking results, summarized in Supplemental Table 1, are shown. These docking results are shown to facilitate visualization of other pol II docking results summarized in Supplemental Table 1, which are described relative to the docking result in B and C. The pol II orientation in B roughly matches that of the activator-bound model shown in A,[1] whereas the pol II orientation shown in C is very different from the activator-bound PIC model. In the Side 1 view, the "X" denotes the pol II stalk domain (RPB4/7) protruding from the structure. Note that the pol II stalk is facing backwards (behind the plane) in C and therefore the "X" is not shown.

Supplemental Table 1. Summary of cross-correlation (CC) values from pol II docking calculations. Eight different pol II crystal structures were docked independently, with PDB files shown at left. Note that PDB 1TWA represents a 10-subunit pol II crystal structure that lacks the RPB4/7 subunits that comprise the stalk domain. The CC value listed is not the actual CC value, but rather is normalized relative to the top CC value for each PDB structure. In every case, the top value corresponded to pol II orientation 1, and the second-highest CC values corresponded to pol II orientation 2. For simplicity, only CC values 0.90 or greater are shown, representing 9 different pol II orientations. Lower CC values (lower than 0.90) mostly represented orientations roughly similar to the 9 shown here; 18 total orientations were observed across all 8 PDB docking experiments, underscoring the variability of pol II orientation in the absence of an activator-Mediator interaction. Only orientations 1 and 2 were represented in all 8 docking experiments. Models based upon these pol II orientations are shown in Supplemental Figure 3B and C.

Supplemental Methods

Purification of Mediator, pol II, and TFIIF

Activator-free Mediator was purified as an endogenous complex from HeLa nuclear extract, as outlined in Figure 1B. Before peptide elution, the anti-MED26 column was washed with 5 times with 10 column volumes of 0.5M KCl HEGN (20 mM HEPES pH 7.9, 0.1 mM EDTA, 10% glycerol, 0.1% NP-40) and once with 10 column volumes 0.15M KCl HEGN (0.02% NP-40). RNA polymerase II was purified from HeLa nuclear extract as described.[1] TFIIF (RAP74 and RAP30) were expressed recombinantly in *E. coli* and purified as described.[11]

Isolation of Mediator–pol II–TFIIF assembly

The Mediator–pol II–TFIIF assembly was prepared essentially as described.[1] In summary, pol II was treated with agarose-conjugated calf intestinal phosphatase (Sigma P0762) for 4h at 4 °C. This dephosphorylated pol II was incubated with an excess of purified TFIIF for 1h at 4 °C. Purified, activator-free Mediator was then mixed with the pol II-TFIIF sample for an additional hour at 4 °C. The Mediator–pol II–TFIIF preparation was applied to a glycerol gradient and centrifuged at 55,000 rpm for 6h at 4 °C.

Antibodies

The western blotting experiment to detect Mediator was completed using an antibody to the 130 kDa Mediator subunit MED23 (Bethyl Cat. # A300-425A). Pol II was detected using an antibody to the N-terminus of RPB1 (Santa Cruz sc-899). TFIIF was detected using an antibody to the RAP74 subunit (Austral Biologicals TM-101D-55).

Electron Microscopy and Image Processing

The Mediator–pol II–TFIIF sample was applied to EM grids and stained with uranyl acetate as previously described.[1] Micrographs were collected using a Tecnai F20 microscope (200 kV) on Kodak SO-163 film. Untilted (0°) and tilted (30°-45°) micrographs were collected for each specimen area at 29,000x magnification with a defocus ranging from -1.0 to -3.2 μm. The film was digitized with a sample-scale pixel size of 4.22 angstroms using a Nikon Super Coolscan 9000 ED.

Negative stain image processing was carried out essentially as described.[1] A total of 13,359 untilted images were classified into two hundred 2D classes. By back-projecting the tilted images for each class, 3D model structures were generated. These 3D structures were cross-correlated using SPIDER[12] and clustered according to their correlation values using the statistical program package R.[13] Two-dimensional classes representing more than 50% of the data clustered together and appeared to represent Mediator–pol II–TFIIF complexes, based upon previous work with VP16-Mediator–pol II–TFIIF.[1] Different subsets of the data from this Mediator–pol II–TFIIF cluster of 2D classes were combined and used to generate a single reference volume, followed by angular refinement. Because the purpose of the negative stain data was to generate a reference volume for refinement with cryo-EM data, only the most homogenous data were used for this analysis. A data set containing 4,252 images was ultimately used to generate a negative stain reference volume with a resolution of 48 Å using the ½-bit information level threshold.[14] This 3D volume was then Butterworth low-pass filtered to 56 Å resolution and used as a reference for the refinement of the Mediator–pol II–TFIIF structure with cryo-EM data.

Additional 3D structures, derived from different and larger subsets of 2D classes of single-particle images, correlated well with the volumes included in this refinement. However, including these data in the refinement caused the density in the central region of the structure to become discontinuous at ~1.8MDa mass thresholds. This indicated that structural heterogeneity or flexibility was likely within this central region compared with other areas of the structure. Of note, similar results were seen in the negative stain data refinement of the VP16-Mediator–pol II binary complex (i.e. without TFIIF). A characteristic feature of these structures was that pol II did not stably orient within the complex,[1] which also was observed with

activator-free Mediator–pol II–TFIIF. Finally, a subset of classes within the negative stain data was observed to correlate well with each other, but poorly with the putative Mediator–pol II–TFIIF classes. Data from these classes appeared to represent Mediator alone (i.e. not bound to pol II–TFIIF) and refinement of this structure was not pursued further.

Cryo-negative stain samples were prepared and image processing was completed essentially as described previously.[1] Cryo grids were imaged using a Tecnai F20 microscope (200 kV) at liquid nitrogen temperature and under low-dose conditions (1000-1500 e/nm^{2}s). Micrographs were recorded on Kodak SO-163 film at 29000x magnification with a defocus ranging from -0.9 to -3.0 μm. The film was digitized with a sample scale pixel size of 4.22 angstroms using a Nikon Super Coolscan 9000 ED scanner. Micrographs were screened for astigmatism and drift as previously described.[1] The program CTFFIND3[15] was used to determine the contrast transfer function parameters for each of the 139 high-quality micrographs. Particle images were selected using Web. Using the Web-generated coordinates, CTF-corrected images were windowed into individual 161x161 pixel boxes using SPIDER. The final cryo-EM data set for Mediator–pol II–TFIIF consisted of 9,169 single-particle images.

The negative stain Mediator–pol II–TFIIF reference structure described above was subjected to projection matching iterative refinement over angular steps of 15°, 10°, 5°, 5°, 4°, and 3°, corresponding to 84, 195, 799, 1253, and 2247 reference projections. A correlation cutoff threshold in which 60% of the full data set was included (5,489 single-particle images) led to the highest resolution 3D structure and did not introduce structural discontinuity. The resolution of this structure was 32 Å, based upon the Fourier Shell Correlation curve[16] or the ½-bit information level threshold.[14]

We also completed additional 3D reconstructions using a multi-reference projection matching refinement protocol.[1,17] This strategy allowed partitioning of the data to one of two reference structures: Mediator–pol II–TFIIF or activator-free Mediator alone.[18] Both complexes were expected to be present within the sample, and this was confirmed upon image processing of the negative stain data (see above). In these experiments, projections of each distinct structure were generated and single-particle images were aligned to the most closely matching projection. This method helped ensure that no images of Mediator alone would be incorrectly incorporated into the structure of Mediator–pol II–TFIIF. No major structural changes in Mediator–pol II–TFIIF were evident upon the completion of this multi-reference refinement procedure, and identical the pol II docking results were observed relative to the "single-reference" refinement described above. This experiment further validated the structure and pol II docking results for the activator-free Mediator–pol II–TFIIF assembly and indicated that unliganded Mediator images were not being incorrectly assigned to projections of Mediator–pol II–TFIIF during single reference refinement.

Pol II crystal structure docking

The yeast pol II crystal structure 1Y1V,[19] with the TFIIS fragment removed, was docked into the Mediator–pol II–TFIIF EM map using the FFT-Accelerated 6D Exhaustive Search program of Situs[20] (version 2.4.3) and Colores,[21] as described.[1] The docking results did not change based upon the initial positioning of the pol II crystal structure. The pol II docking results were confirmed using other 12-subunit yeast pol II crystal structures, including 1NT9, 1PQV, 1WCM, 2B63, 3FKI, and 3HOZ. Additionally, the same docking results were obtained when using a 10-subunit pol II crystal structure (1TWA)[22] that lacked the pol II stalk subunits RPB4 and RPB7. In Situs, we used the Laplacian filter for these lower resolution structures; whereas this method improves docking precision, the CC values are much smaller and similar compared with a standard linear cross-correlation.[21] Lower values were also a consequence of the resolution (32 Å) and that pol II represents less than 30% of the entire assembly structure. As a result, this method minimizes the ability to reliably discriminate docking fits using CC values only. Thus, we completed independent docking with multiple different PDB files as a means to better evaluate the fits. Consistent with variable orientations of pol II in the activator-free Mediator-pol II-TFIIF structure, several fits yielded similar CC values. Because the pol II stalk and cleft could not be resolved in the activator-free structure, we could not use these structural features as an additional means to evaluate the docking results. These problems were overcome with the VP16-Mediator-pol II-TFIIF structure,[1] in part because both the stalk and the cleft were clearly

resolved in the 3D cryo-EM map and could therefore be used to verify the consistent best docking fits obtained with different PDB files.

3D variance analysis

The 3D variance within the refined Mediator–pol II–TFIIF cryo-EM structure was calculated as described,[1,23] using focused classification within the area of peak variance (Fig. 3C). Generation of two Mediator–pol II–TFIIF substructures based upon partitioning the data with this focused classification protocol yielded two similar 3D structures, each of which resembled the original refined Mediator–pol II–TFIIF structure shown in Figure 3A (data not shown). Furthermore, the pol II docking calculations again revealed a similar distribution of pol II orientations (e.g. Supplemental Table 1), with the top-correlating orientations being identical to those shown in Supplemental Figure 3B and 3C.

Supplemental References

1. Bernecky, C., Grob, P., Ebmeier, C. C., Nogales, E. & Taatjes, D. J. (2011). Molecular architecture of the human Mediator-RNA polymerase II-TFIIF assembly. *PLoS Biol.* **9**, e1000603.
2. Chen, H., Warfield, L. & Hahn, S. (2007). The positions of TFIIF and TFIIE in the RNA polymerase II transcription preinitiation complex. *Nat Struct Mol Biol* **14**, 696-703.
3. Kim, T., Ebright, R. H. & Reinberg, D. (2000). Mechanism of ATP-dependent promoter melting by transcription factor IIH. *Science* **288**, 1418-1421.
4. Kostrewa, D., Zeller, M. E., Armache, K., Seizl, M., Leike, K., Thomm, M. & Cramer, P. (2009). RNA polymerase II-TFIIB structure and mechanism of transcription initation. *Nature* **462**, 323-330.
5. Liu, X., Bushnell, D. A., Wang, D., Calero, G. & Kornberg, R. D. (2010). Structure of an RNA polymerase II-TFIIB complex and the transcription initiation mechanism. *Science* **327**, 206-209.
6. Miller, G. & Hahn, S. (2006). A DNA-tethered cleavage probe reveals the path for promoter DNA in the yeast preinitiation complex. *Nat Struct Mol Biol* **13**, 603-610.
7. Andel, F., 3rd, Ladurner, A. G., Inouye, C., Tjian, R. & Nogales, E. (1999). Three-dimensional structure of the human TFIID-IIA-IIB complex. *Science* **286**, 2153-6.
8. Chen, Z. A., Jawhari, A., Fischer, L., Buchen, C., Tahir, S., Kamenski, T., Rasmussen, M., Lariviere, L., Bukowski-Wills, J., Nilges, M., Cramer, P. & Rappsilber, J. (2010). Architechture of the RNA polymerase II-TFIIF complex revealed by cross-linking and mass spectrometry. *EMBO J* **29**, 717-726.
9. Eichner, J., Chen, H., Warfield, L. & Hahn, S. (2010). Position of the general transcription factor TFIIF within the RNA polymerase II transcription preinitiation complex. *EMBO J* **29**, 706-716.
10. Chen, H. T. & Hahn, S. (2004). Mapping the location of TFIIB within the RNA polymerase II transcription preinitiation complex: a model for the structure of the PIC. *Cell* **119**, 169-180.
11. Knuesel, M. T., Meyer, K. D., Bernecky, C. & Taatjes, D. J. (2009). The human CDK8 subcomplex is a molecular switch that controls Mediator co-activator function. *Genes & Development* **23**, 439-451.
12. Frank, J., Radermacher, M., Penczek, P., Zhu, J., Li, Y. H., Ladjadj, M. & Leith, A. (1996). SPIDER and WEB: Processing and visualization of images in 3D electron microscopy and related fields. *J. Struct. Biol.* **116**, 190-199.
13. Team, R. D. C. (2005). R: A language and environment for statistical computing. In *R Foundation for Statistical Computing*, Vienna, Austria.
14. van Heel, M. & Schatz, M. (2005). Fourier shell correlation threshold criteria. *J Struct Biol.* **151**, 250-262.
15. Mindell, J. A. & Grigorieff, N. (2003). Accurate determination of local defocus and specimen tilt in electron microscopy. *J Struct Biol.* **142**, 334-347.
16. Bottcher, B., Wynne, S. A. & Crowther, R. A. (1997). Determination of the fold of the core protein of hepatitis B virus by electron cryomicroscopy. *Nature* **386**, 88-91.
17. Grob, P., Cruse, M. J., Inouye, C., Peris, M., Penczek, P., Tjian, R. & Nogales, E. (2006). Cryo-

electron microscopy studies of human TFIID: conformational breathing in the integration of gene regulatory cues. *Structure* **14**, 511-520.
18. Taatjes, D. J., Naar, A. M., Andel, F., Nogales, E. & Tjian, R. (2002). Structure, function, and activator-induced conformations of the CRSP coactivator. *Science* **295**, 1058-1062.
19. Kettenberger, H., Armache, K. & Cramer, P. (2004). Complete RNA polymerase II elongation complex structure and its interactions with NTP and TFIIS. *Mol Cell* **16**, 955-965.
20. Wriggers, W. (2010). Using Situs for the integration of multi-resolution structures. *Biophys Rev* **2**, 21-27.
21. Chacon, P. & Wriggers, W. (2002). Multi-resolution contour-based fitting of macromolecular structures. *J. Mol. Biol.* **317**, 375-384.
22. Westover, K. D., Bushnell, D. A. & Kornberg, R. D. (2004). Structural basis of transcription: nucleotide selection by rotation in the RNA polymerase II active center. *Cell* **119**, 481-489.
23. Penczek, P., Yang, C., Frank, J. & Spahn, C. M. (2006). Estimation of variance in single-particle reconstruction using the bootstrap technique. *J. Struct. Biol.* **154**, 168-183.

S Figure 1

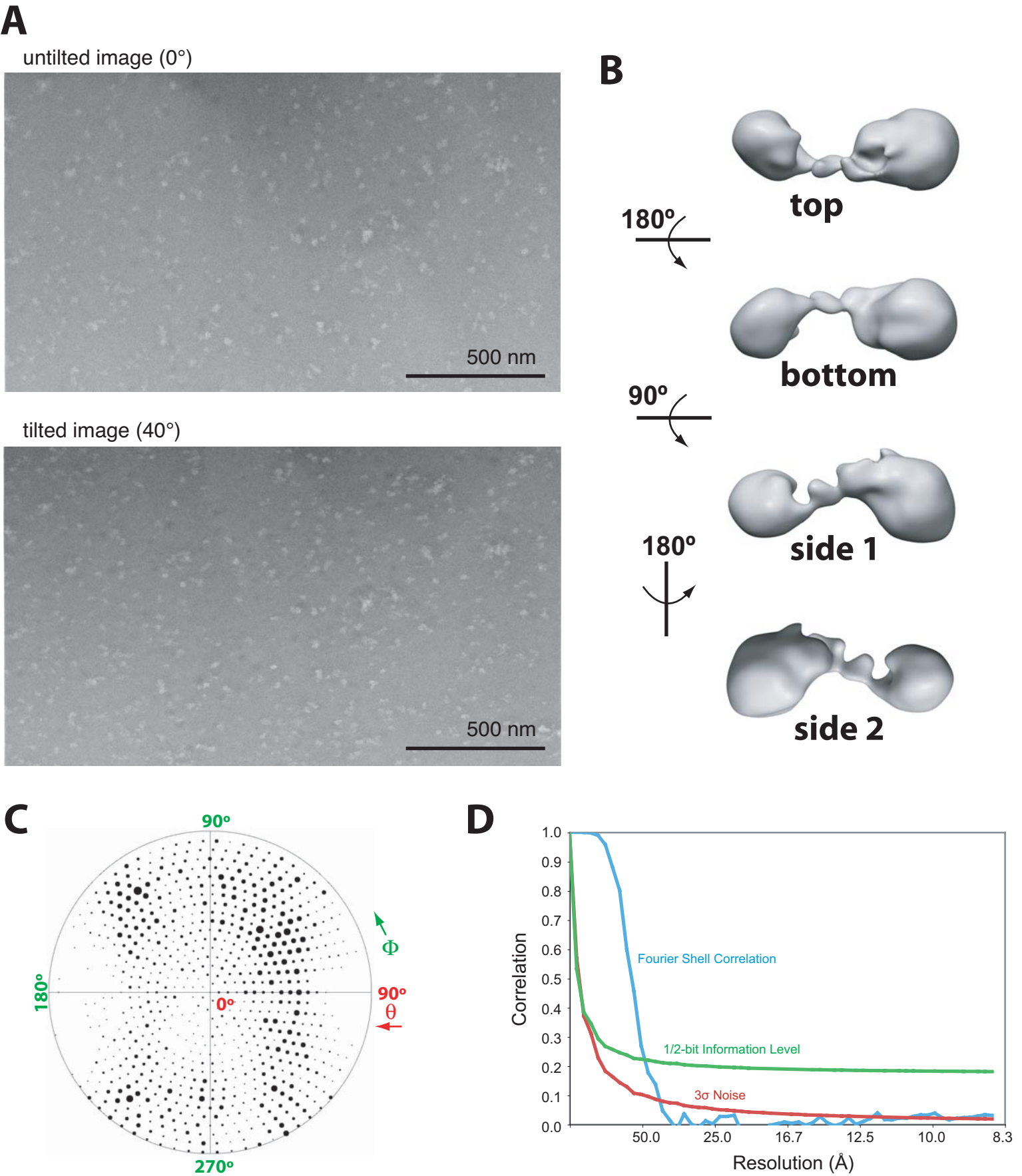
A
untilted image (0°)
500 nm
tilted image (40°)
500 nm
B
top
180°
bottom
90°
side 1
180°
side 2
C
90°
180°
0°
90°
θ
Φ
270°
D
Correlation
1.0
0.9
0.8
0.7
0.6
0.5
0.4
0.3
0.2
0.1
0.0
Fourier Shell Correlation
1/2-bit Information Level
3σ Noise
50.0
25.0
16.7
12.5
10.0
8.3
Resolution (Å)

S Figure 2

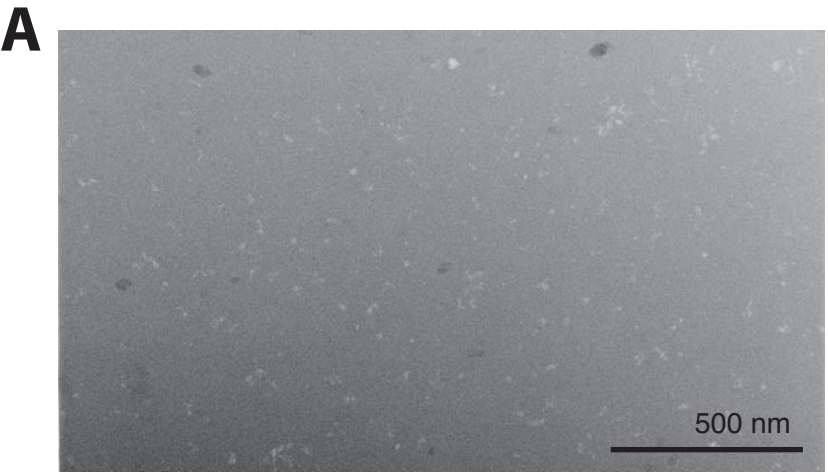
A
500 nm

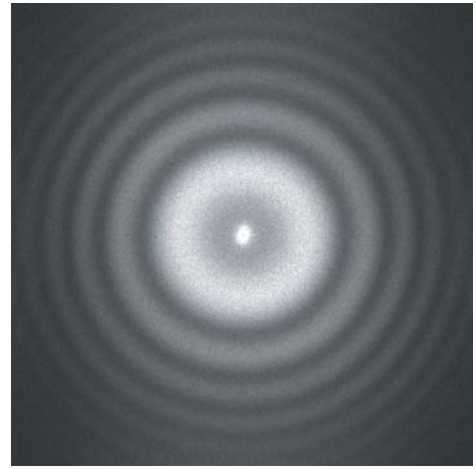
B

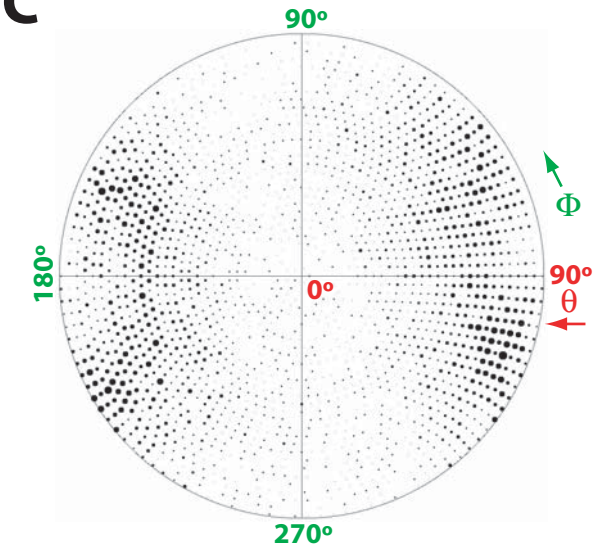
C
90°
Φ
180°
0°
90°
θ
270°

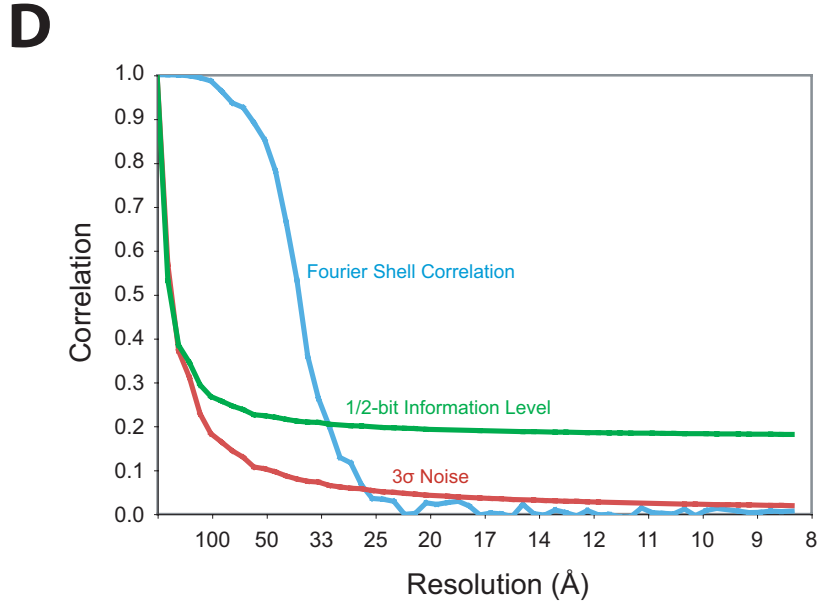
D
1.0
0.9
0.8
0.7
0.6
0.5
0.4
0.3
0.2
0.1
0.0
Correlation
Fourier Shell Correlation
1/2-bit Information Level
3σ Noise
100
50
33
25
20
17
14
12
11
10
9
8
Resolution (Å)

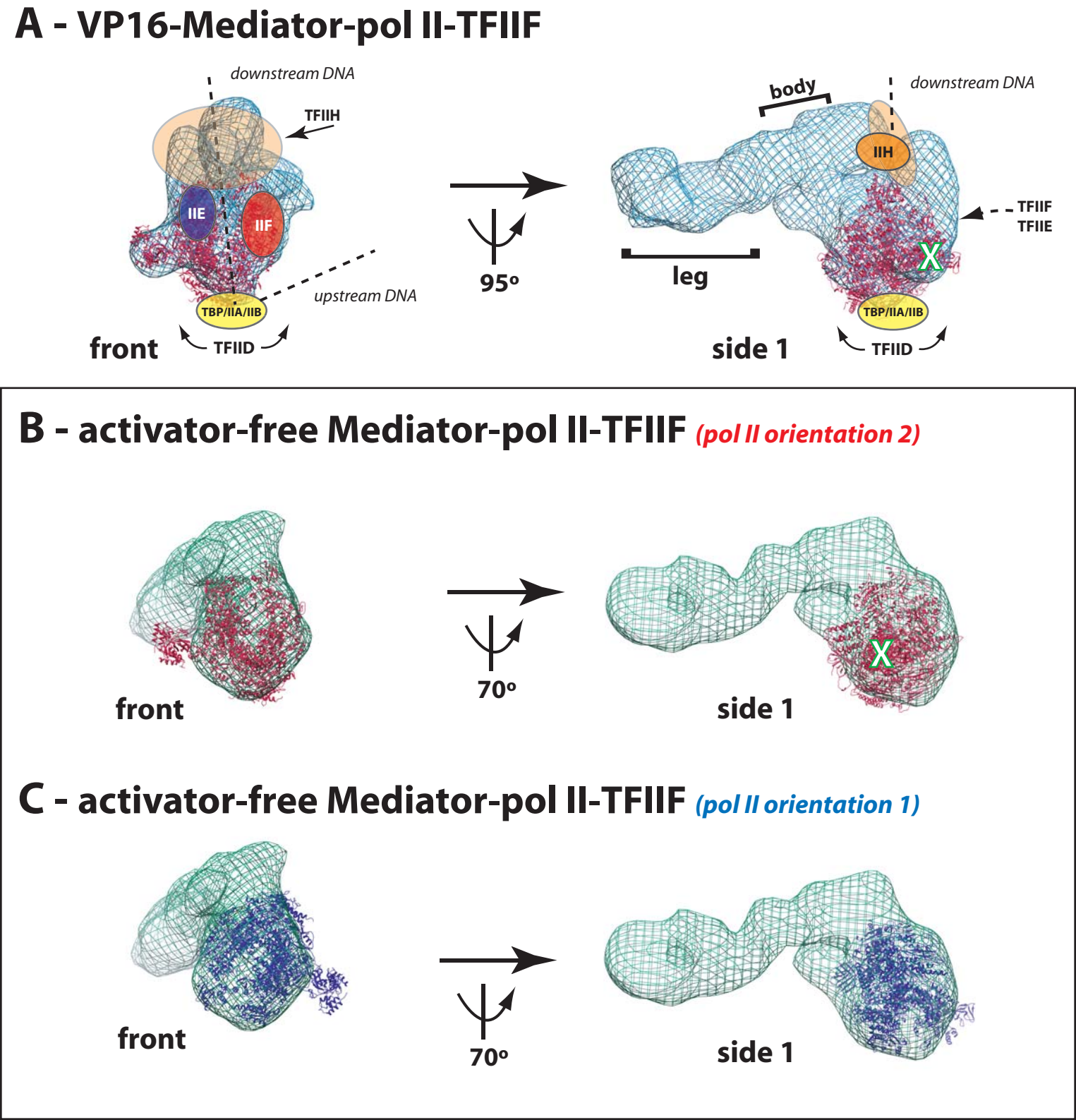
A - VP16-Mediator-pol II-TFIIF
downstream DNA
TFIIH
IIE
IIF
upstream DNA
TBP/IIA/IIB
TFIID
front
95°
body
downstream DNA
IIH
TFIIF
TFIIE
X
leg
TBP/IIA/IIB
TFIID
side 1
B - activator-free Mediator-pol II-TFIIF (pol II orientation 2)
front
70°
X
side 1
C - activator-free Mediator-pol II-TFIIF (pol II orientation 1)
front
70°
side 1

	Pol II orientation 1	Pol II orientation 2		Orientation 3	Orientation 4	Orientation 5	Orientation 6	Orientation 7	Orientation 8	Orientation 9
1Y1V	**1.00**	**0.96**		0.96	0.92	0.90	0.90			
1NT9	**1.00**	**0.95**		0.95						
1PQV	**1.00**	**0.97**		0.96	0.91					
1TWA	**1.00**	**0.94**							0.90	
1WCM	**1.00**	**0.96**			0.91			0.90		0.90
2B63	**1.00**	**0.94**		0.95	0.91	0.91		0.90		
3FKI	**1.00**	**0.94**			0.90					
3HOZ	**1.00**	**0.95**		0.95	0.90			0.90		
Average	**1.000000**	**0.950994**								
Percent	**100%**	**95%**								